Advanced Sciences and Technology Journal

ASTJ vol. 2, no. 2 (2025), P 1052
10.21608/astj.2025.357163.1052
https://astj.journals.ekb.eg/

Characterization of Geopolymer Concrete Incorporating GGBFS and FA as Binding Materials

Karim Mohsen, Khalid M. Morsy, Ibrahim A. Yousif and Ehab F. Sadek

Structural Engineering Department, Faculty of Engineering, Ain Shams University, Cairo, Egypt

A R T I C L E I N F O

Article history:
Received 1 February 2025
Revised 19 February 2025
Accepted 19 February 2025
Available online 19 March 2025

Handling Editor:
Prof. Dr. Mohamed Talaat Moustafa

Keywords:
Geopolymer concrete (GPC)
Conventional Concrete (CC)
Alkali activation
Fly Ash
Mechanical properties

A B S T R A C T

Portland cement is the primary binding ingredient used in the creation of concrete, which is one of the factors thought to be one of the main causes of global warming. Several alternatives have been proposed to reduce the environmental impact of concrete manufacturing as it has been found that the cement industry is responsible for about 8% of global CO_2 emission. In recent years, alkali-activated binder, a new environmentally friendly inorganic binder made by activating alumino-silicate source material with an alkaline solution, has gained a lot of attention as a viable alternative to Portland cement. Despite the fact that a good assessment of the mechanical properties of geopolymer concrete (GPC) is required for the appropriate design of concrete structural members and the retrofitting of ordinary Portland concrete structures, there are few test results available in the literature. The current study aimed to provide essential information for future development and understanding of the mechanical properties and behavior of GPC as a retrofitting material for reinforced concrete deteriorated structures. The fresh and hardened state properties of both Portland cement concrete and GPC include slump loss, compressive strength (fc), flexural strength (fr), tensile strength (ft), modulus of elasticity (E), stress-strain relationship, bond strength with RFT bars, drying shrinkage, coefficient of thermal expansion tests were performed. The microstructure was also examined. The mechanical results achieved for GPC validated its potential as a high-performance repair material suitable for damaged concrete structures.

1. INTRODUCTION

1.1. Environmental impact of ordinary Portland cement concrete

The largest problem in combating climate change is the manufacture of cement, which is regarded the basic element of Portland Cement Concrete (PCC), which accounts for around 10-12% of total concrete volume, and the world's desire for it appears insatiable. The demand for Portland cement (PC) has recently surged, leading in an increase in production, with a global PC production now exceeding 3 billion tons per year [1] and the demand for PCs is anticipated to surpass 6 billion tons annually over the next four decades. Fig 1 shows the global cement production in the year 2018.

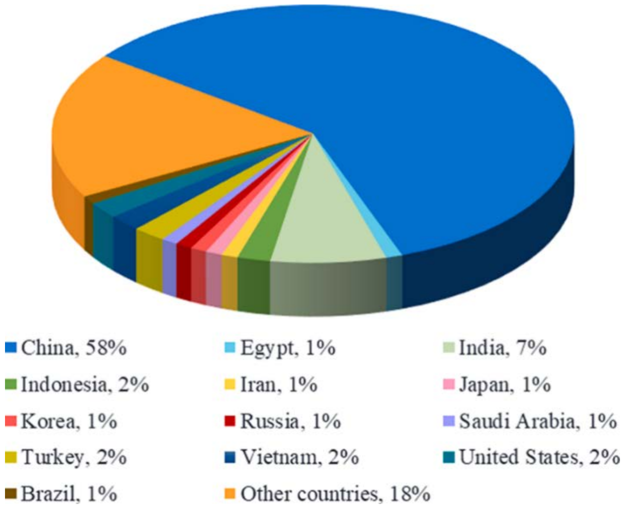

Fig 1. Production of cement around the world (U.S. Geological Survey 2018)

The PCC serves as the backbone of the construction industry. In a rotating kiln, limestone or chalk is heated alongside clay to an elevated temperature of approximately 1450 °C. This process results in the formation of hard clinker nodules, which are subsequently ground with a small amount of gypsum. In the combustion process, coal or petroleum coke is heavily utilized as fuel. The primary environmental hazards associated with PCC production involve swift landscape degradation, dust buildup during transport, and noise pollution during quarrying and processing of raw materials. Hutchinson et al. [2] claimed, "The production of PCC involves the emission of considerable CO2, which occurs in two phases: firstly, by burning fuel to achieve the high temperatures required in kilns, and secondly, through a calcining reaction that takes place as limestone is heated." Additionally, the production of Portland cement is an energy-demanding industry, where energy represents approximately 50 - 60% of overall manufacturing expenses [3]. The production of Portland cement demands a large amount of electrical and thermal energy; for instance, creating one ton of clinker consumes around 110 - 120 kWh and roughly 3000 - 6500 MJ [4]. The average usage of electrical and thermal energy for Portland cement manufacturing across different countries is shown in Fig 2 [5].

PCC has also struggled in acid or sulfate environments, particularly in marine structures. Due to its calcium content, PCC is susceptible to acid erosion. Calcium substances dissolve rapidly in an acidic setting, leading to heightened porosity and swift breakdown [6]. Certainly, several existing OPC structures that have developed over the years are encountering an inevitable phase of disintegration [7]. Certainly, the longevity of OPC is undoubtedly associated with the properties of its components, which consist of roughly 60-65% CaO and about 25% $Ca(OH)_2$ in the product of its hydration. Because of the aggressive reactivity of $Ca(OH)_2$ in acidic environments, OPC is ineffective at retaining water. Additionally, when CO_2 reacts with $Ca(OH)_2$, it swiftly deteriorates OPC-based concrete or mortars [7]. The corrosion of reinforcement contained in OPC significantly affects the product's service life cycles, durability, design duration, and safety. Due to the significant drawbacks of OPC, researchers opted to explore a feasible solution that could serve as a practical alternative to conventional concrete, ensuring both environmental sustainability and structural durability.

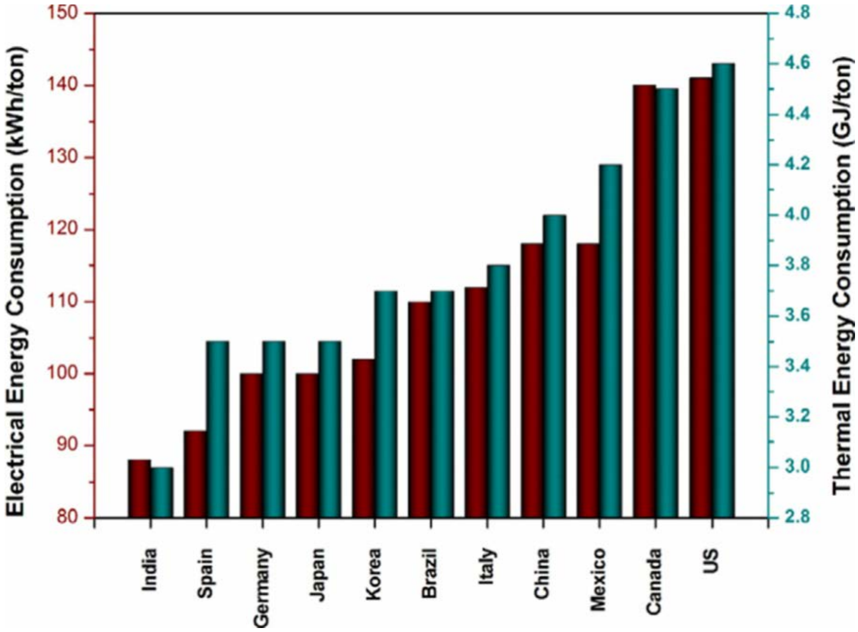

Fig 2. Required Electrical and thermal energy consumption for producing Portland cement for various countries [5]

CO_2 emissions may be decreased through several methods, such as (1) substituting cement with secondary raw materials and secondary cementitious substances, (2) employing alternative fuel during clinker cement production, (3) utilizing alternative binders in concrete production, and (4) diminishing process-related emissions by altering the manufacturing approach [8]. Utilizing alternative binders and raw materials in concrete production could greatly reduce CO_2 emissions. These alternative binders can decrease gases without compromising cement properties, while also improving the performance of cement mortar.

It was investigated that usage of geopolymer may decrease the amount of emissions of carbon dioxide by up to 64 % compared to the use of cement [9]. Moreover, from an economic view, the price of source materials is lower than cement, for example, the price of GPC which depended on fly ash as aluminosilicate material is cheaper than conventional concrete by 10-30% after taking into consideration the price of alkaline activator [10]. According to a review of the literature, geopolymers have shown high mechanical strength and durability. High early strength, resistance to high temperatures, and high performance in acid and sulphate environments. These characteristics make geopolymer a viable alternative for a wide range of industrial applications, including civil engineering, automotive and aerospace, nonferrous foundries and metallurgy, plastics, waste management, art, and decoration, and building retrofitting.

1.2. Literature Review

GPC (GPC) is high in aluminosilicate and has characteristics similar to cement because these GP composites are unreactive in the presence of water, they require an alkaline media to work properly [11]. Furthermore, when combined with an alkaline binder, these GPs alternative binders can support load by forming a 3-D polymeric structure. The cement component reacts quickly with water because to its high natural alkaline concentration [11]. In order to form a binding with the neighboring matrix, an alkaline binder must be activated in an alkaline media.

1.2.1. Compressive Strength (f_c)

The f_c of conventional concrete is the key mechanical property, as ultimate strength is vital for construction materials. Additional concrete properties like f_r, f_t, and E are closely associated with f_c.

Heat-cured GPC attains complete f_c within one day. Almost 90% of the strength can be attained within hours when cured at temperatures between 80 and 90 °C. Conversely, GPC cured under ambient conditions enhances strength over time just as PCC does. Every curing condition leads to enduring strength, and the curing temperature merely affects the duration required to reach the ultimate f_c of a specific mix.

Numerous aspects affect GPC strength, such as the binder's calcium content, the type and quantity of alkaline activator, the molarity of the activator, the ratio of binder to aggregate, and the ratio of liquid to solid. Additionally, the source material, curing conditions, and particle-size distribution all significantly influence the evolution of GPC f_c.

Ismail et al. [12] assessed the initial f_c of GPC using metakaoline (MK) and fly ash (FA) as raw materials and varied ratios of Na_2SiO_3 and NaOH solution. FA composition, surface area, and particle morphologies all influence GPC f_c [13]. It was found out that, increasing the Al/Si ratio above two slows down the geopolymerization process and reduces the initial f_c of GPC [12].

Husein et al. [14] created GPMs by substituting MK with ground granulated blast furnace slag (GGBFS) at concentrations ranging from 0% to 15%. It was discovered that, after 28 days of curing, the f_c of the resulting GPM rose from 42 to 63.1 MPa, with an increase in MK content of 10-15%, respectively as a substitute for GGBFS. Husein et al. [15] investigated how the calcium to silicate ratio in the binder influenced strength development at different curing temperatures. The f_c lessened with lower calcium content and decreased curing temperature. The weakest strength was achieved with a calcium to silicate ratio of 1.08 under oven curing conditions at 90 °C.

Tanakon et al. [16] investigated the effect of different NaOH molarities (6, 10, and 14 M) on GPM f_c growth. The results showed that as the molarity of NaOH grew, so did the f_c. Vasconcelos et al. [17] studied the effect of different NaOH concentrations (12, 14, and 16 M) on the growth of GPM strength. After 7, 28, and 56 days, the f_c was raised by increasing the NaOH content from 12 M to 14 M. However, strength decreased after 14 M. The strength was found to be lower at 16 M than at 14 M.

1.2.2. Stress – strain relationship (SSR)

Thomas and Peethamparan [18] published the experimental curves of SSR of GPC, which were compared to numerically calculated PCC curves [19]. It was discovered that the GPC exhibits brittle failure after promptly reaching the peak. The widespread micro cracking in GPC explains its extreme brittleness [20]. As a result, it was determined that GPC has higher brittleness than PCC as illustrated in Fig 3.

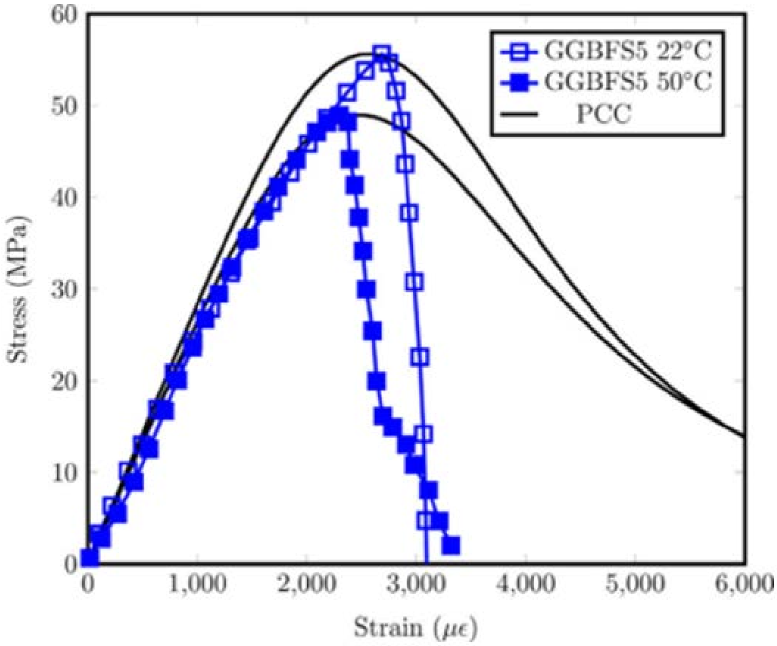

Fig 3. Representative SSR curves for GPC [18]

Ding et al. [21] analyzed the SSR identified by Yang et al. [22] alongside Thomas and Peethamparan [18], as illustrated in Fig 4. Similar to PCC, the f_c significantly influences the SSR of GPC, affecting both the initial stiffness and the peak strain. The CIB-FIP model does not align with the SSR of GPC, as it predicted lower values for the ascending branch and higher for the descending branch, indicating that GPC exhibits greater ductility than PCC at identical f_c [22]. This aligned with the findings of Thomas and Peethamparan [18] regarding the ascending section, but the obtained descending part exhibited greater brittleness (i.e., a quicker decline).

1.2.3. Modulus of elasticity (E)

Ding et al. [21] examined the relation between f_c and E which is shown in Fig 5 reported by Douglas et al. [23], Yang et al. [22], and Thomas and Peetham-paran [18]. Also, the relationships that predicted by CEB-FIP model, ACI 318 and the generated equation by Yang et al. [22] are compared on the same figure. Douglas et al. [23] reported that ACI code 318 can predict the E of GPC. Similarly, Yang et al. [22] concluded that the E of GPC activated by $Ca(OH)_2$ can be approximated using ACI code 318. Thomas and Peethamparan [18] recorded that the E of GPC varied slightly with the f_c and the ACI code 318 fit the obtained experimental results poorly.

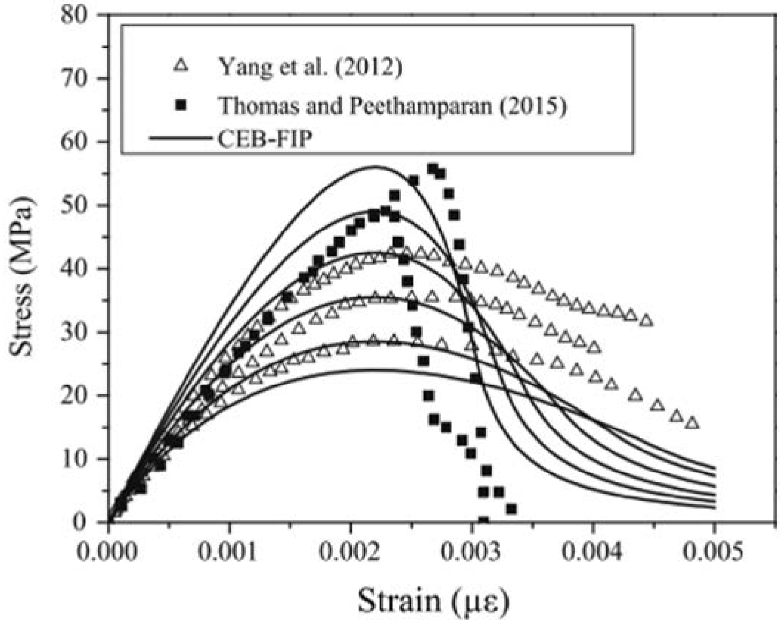

Fig 4. SSR curves for GPC [18]

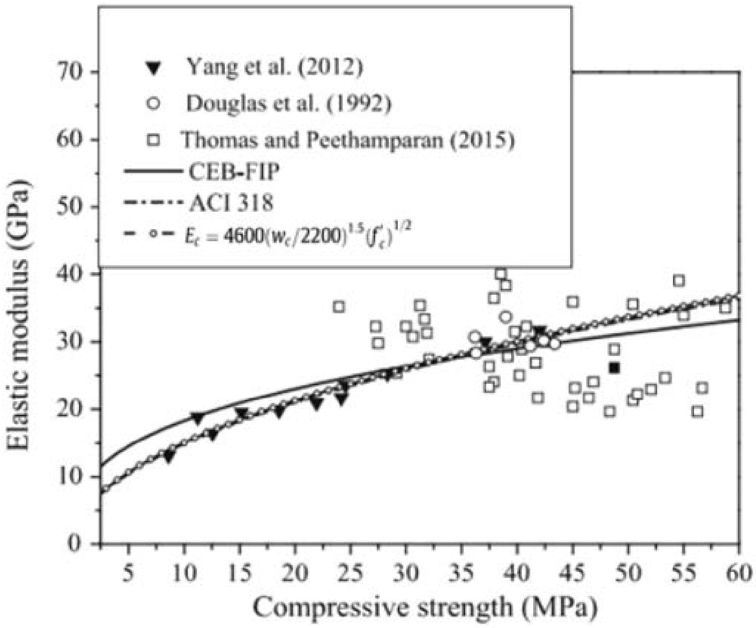

Fig 5. Relation between E and f_c of GPC and PCC [18]

Aliabdo et al. [24] came to the conclusion that the relationship between E and f_c for GPC can be represented by the following equation. As shown in Fig 6, this relationship was derived from the results of testing 27 mixes.

$$Ec = 3.726\sqrt{CS} \tag{1}$$

where, E is modulus of elasticity in GPa, and CS is f_c in MPa.

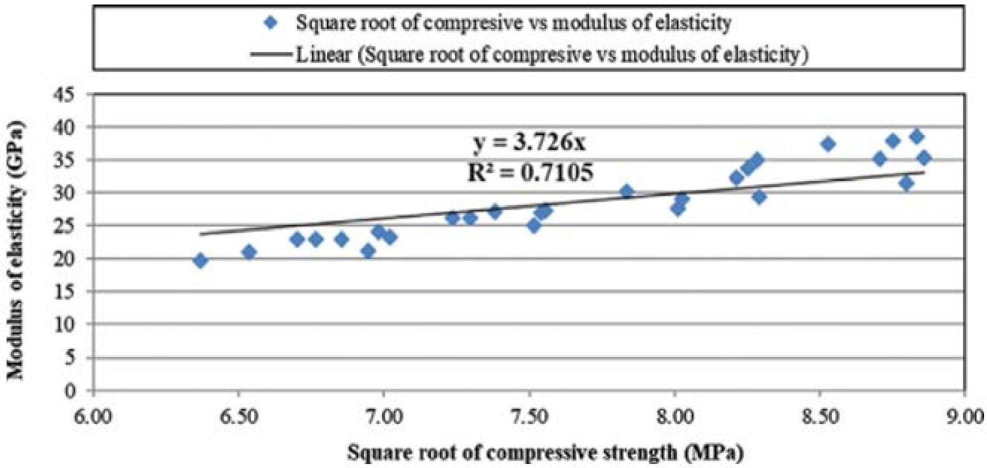

Fig 6. Relation between square root of f_c and E of GPC [18]

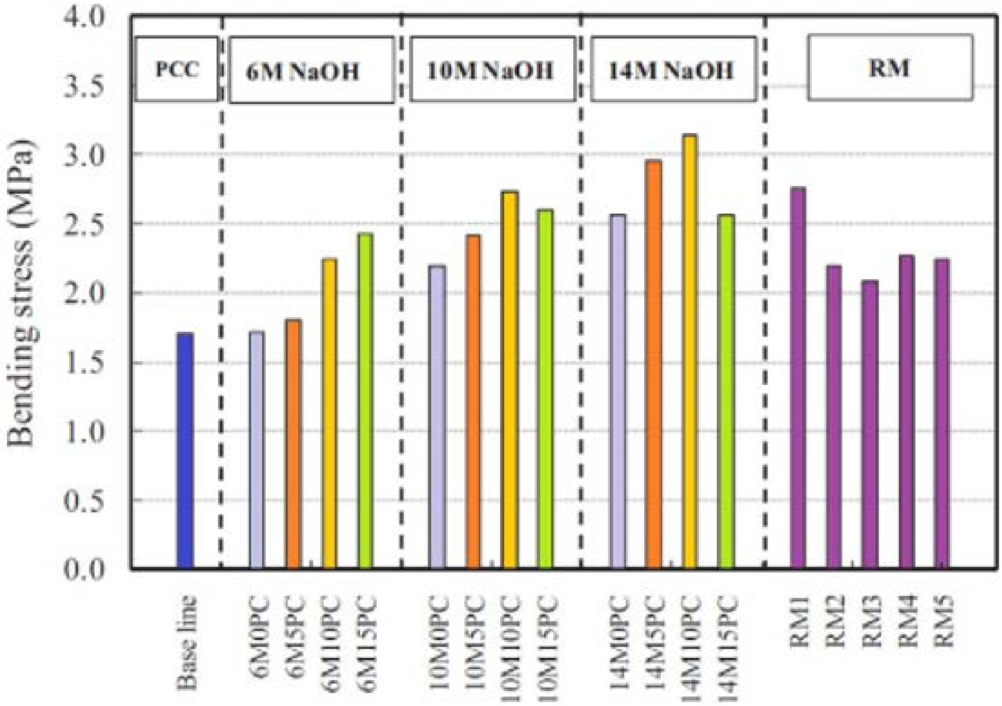

Fig 7. Bending stress of PCC notched beam with GPM or RM as repair materials [18]

1.2.4. *Flexural Strength (f_r)*

The f_r of GPM used as repair materials was examined by Phoo-ngernkham et al [16]. High content calcium materials (HFA) and PCC were employed with different molarities of the alkali activator solution. Figure 7 shows the bending stresses of notched PCC beams filled with GPM or RM. The bending stress of the PCC notched beam rose with higher PC content, due to a rise in reaction products and related enhancements in GPM strength and adhesion ability. This led to a general decrease in the bending stresses of PCC notched beams. The bending stress (3.1 MPa) of the notched beam filled with GPM (10% PC) and treated with 14 M of NaOH was favorable, showing about an 85% enhancement over the baseline. In combinations with elevated NaOH concentrations, the interaction between NaOH and the PCC substrate in the transition zone was noted to enhance performance. This assessment verified the suitability of PC integrated GPM as a viable repair option.

1.3. Study Objectives

The idea behind the engineering design process is to employ the optimums to achieve the goal; choosing the optimum material is based on criteria such as durability, material cost, maintenance cost, and environmental impact. The researchers were driven to develop answers to the problem by the durability and environmental pollution issues associated with the production of cement, which is employed as the principal binder in PCC. Geopolymer (GP) composite is one of the major solutions for finding an alternative to PCC concrete. GPC, which is created from diverse waste products and has a significant quantity of Al_2SiO_3 and Na_2SiO_3/NaOH (alkali-activated silica), is emerging as an important material for sustainability. It is also preferred since it emits less pollution.

A variety of research has been carried out in recent years to enhance the strength of geopolymer materials, examine the properties of geopolymer in both fresh and hardened states, and understand the geopolymerization process. Nonetheless, most of these studies focused on paste and mortar instead of concrete. The current research aimed to offer fundamental information regarding the mechanical characteristics of GPC that includes GGBFS and FA as binding agents.

2. Experimental Program

2.1. Material Characterization

GPC was produced using cementless binder, pure GGBFS and FA were employed as constituents. Because they possessed both cementitious and pozzolanic properties, the slag binder (off-white in appearance) stood out among the other supplementary cementitious compounds. X-Ray fluorescence (XRF) test was performed to investigate the chemical compositions of GGBFS which is made of calcium (37.50%), silicate (35.10%), and alumina (16.90%). The Fly ash binder with a low calcium content was also used as another constituent in preparation of GPCs. The FA (grey in appearance) is made of calcium (1.90%), silicate (53.50%), and alumina (27.80%), according to X-Ray fluorescence

(XRF) test. Sodium hydroxide solution (NaOH) (60.25% Na_2O, and 39.25% H_2O) and sodium silicate solution (11.98% Na_2O, 31.00% SiO_2, and 57.00% H_2O) were used as liquid activators. Ordinary Portland cement concrete was produced using cement as the main binder while the activator was only by using water to form hydration products. Table 1 summarizes the composition of GGBFS, FA and Portland cement using X-Ray fluorescence (XRF) test. The locally available natural sand with a nominal maximum particle size of 5 mm and the crushed with a nominal maximum size of 10 mm were used for fine aggregate and coarse aggregate, respectively. The specific gravity was 2.62 for fine aggregate while specific gravity and water absorption were 2.60 and 0.98%, respectively, for coarse aggregate. Table 2 summarizes the physical and chemical properties of used fine and coarse aggregate which met the standard recommendations in ASTM C33.

Table 1 Chemical composition of GGBFS, FA and PC

Materials	SiO_2	Al_2O_3	CaO	MgO	Fe_2O_3	MnO	TiO_2
GGBFS	35.10	16.90	37.50	7.85	1.30	0.52	0.23
FA	53.50	27.80	1.90	0.90	11.20	0.20	3.20
PC	19.02	4.34	63.25	0.77	3.45	0.26	0.28

GGBFS: Ground Granulated Blast Furnace Slag
FA: Fly Ash
PC: Portland cement

Table 2 Chemical and physical properties of fine and coarse aggregate

Materials	NMS (mm)	Unit Weight (kg/m^3)	Specific Gravity	Water Absorption (%)	Fine Material Content (%)	Chloride Content (%)	Sulphate Content (%)
Fine Aggregate	5	1590	2.62	--	2.40	0.0285	0.1453
Coarse Aggregate	10	1550	2.60	1.50	0.46	0.0137	0.2957

2.2. Mixtures Proportions

Two types of industrial waste materials (FA and GGBFS) were used to prepare the GPC mix design. The water-to-FA or GGBFS, alkaline-to-FA or GGBFS, SS/SH and all other factors affecting the mix design of GPC were selected based on a comprehensive trial mixture [25]. All aggregates were batched in a saturated surface dry state. The quantities of the PCC mixture were chosen to provide a f_c of 28 days comparable to that of the geopolymer mixture. Also, the water-to-binder ratio was kept constant in the three mixes taking into consideration the water in the alkaline activator in GPC mixes. Table 3 summarizes the mix proportions of two GPC mixes and one Portland cement concrete mix which were prepared during the course of this study.

Table 3 Mix proportions of GPC and PCC (kg/m^3)

Mixes	GGBFS	FA	PC	Na_2SiO_3	NaOH	Water	W/B	F.A	C.A	Admixture (%)
SGC	450	0	0	131	41	112	0.45	547	1093	0
FSGC	270	180	0	131	41	112	0.45	547	1093	0
PCC	0	0	450	0	0	198	0.45	703	1055	1

SGC: Slag-based geopolymer concrete.
FSGC: (Fly ash + slag) based geopolymer concrete.
PCC: Portland cement concrete.
W/B: Water to binder ratio.
F.A: Fine Aggregate.
C.A: Coarse Aggregate.
Admixture: water-reducing agent and super- plasticizer.

2.3. Concrete Manufacturing

The process of blending GPC carried out in this study began with combining the dry components (GGBFS or FA and aggregates) in the pan mixer for 1 minute. Next, incorporate the alkaline activator into the dry blend and mix for approximately 4 minutes, or until the mixture becomes uniform. Prior to incorporating the alkaline activator into the dry mixture, the SH pullets, SS solution, and water were blended for roughly 1 hour. After 24 hours, the samples were taken out of the moulds and cured in the laboratory at a temperature of 25±2 oC for GPC mixtures and in water curing tanks for PCC mixtures until evaluation.

3. Results and discussion

3.1. Slump Loss

The workability of fresh GPC and PCC mixes was detected by slump loss test according to ASTM C143 standard [26]. The slump tests were conducted immediately after mixing and at fixed time intervals to measure the workability of all mixes with time. GPC mixtures have a higher initial slump but lesser workability over time than Portland cement concrete mixes. Fig 8 depicts the slump loss measurements of all the three mixes implemented in this study. Fig 9 shows that, as the GGBFS content increased, the workability of the concrete decreased due to the quick pace of chemical reaction. As a result, boosting the GGBFS level (100%) reduced the mix's workability. Reducing the GGBFS proportion and raising the FA level (GGBFS 60% & FA 40%) enhanced the workability of the mix as time progressed. This aligns with the results of an earlier study carried out by Al-Majidi et al. [34]. This is probably a result of variations in the physical characteristics and chemical interactions of the mixtures. With an increase in GGBFS content, the quantity of angular particles rises while the amount of spherical particles from FA decreases. The round shape can enhance the Flowability of the concrete mix. Furthermore, combining GGBFS and FA provides additional reactive material, resulting in quicker setting and decreasing workability.

Fig 8. slump loss test measurements

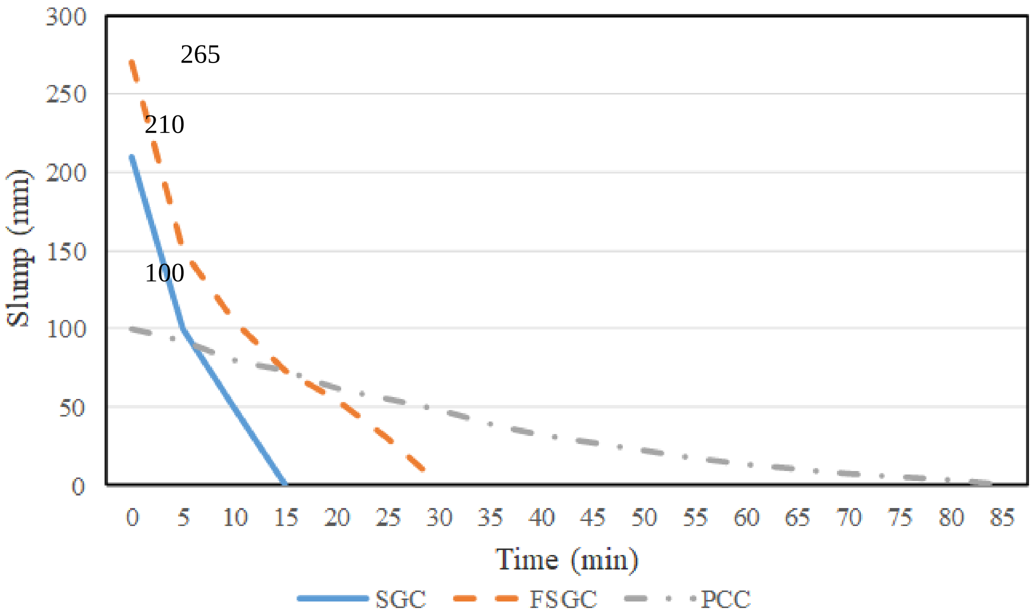

Fig 9. Slump loss test results

3.2. Compressive Strength Development

f_c test was conducted on 100×100×100 mm cubic specimens after 1,3,7,28, and 90 days from casting according to BS EN 12390-3 [27]. The highest f_c after 28 days was achieved by mix (SGC) (100% GGBFS), which was about 60.0 MPa. The (FSGC) mix and (PCC) mix achieved f_c after 28 days of 49.0 MPa and 43.0 MPa respectively as illustrated in Fig 10. The specimens prepared with (40% FA & 60% GGBFS) presented a lower f_c than specimens prepared with (100% GGBFS) by a percentage of almost 20% after 28 days. The incorporation of a greater quantity of GGBFS showed a beneficial impact on the f_c of the concrete samples. With an increase in the GGBFS content, the initial f_c of the samples rose, reaching 29.7 MPa at 24 hours, in contrast to the 20.3 MPa obtained with 40% FA. Comparable patterns in the development of f_c were noted at the ages of 3-, 7-, 28-, and 90-days during curing at room temperature. This was discovered to agree with the results of Tanakorn et al. [35] and Sanjay et al. [36]. The improvement in f_c alongside the increase in GGBFS content was linked to the rise in CaO levels and the decrease in SiO_2 concentrations within the concrete matrix. Additionally, a rise in the GGBFS content resulted in a high ratio of CaO to SiO_2 reaching 0.95, which contributed to the development of more C-(A)-S-H gel in the concrete mixtures [15], [37]. Three essential processes were introduced to explain the influence of GGBFS on gel creation. The initial factor was enhanced f_c attributed to a higher formation rate of C–S–H gel caused by the introduction of dissolved Ca on the surface of GGBFS. It was acknowledged that the higher rate of C–S–H formation with Ca could lead to a water deficit in the mortar matrix and elevate its alkalinity, thereby enhancing the dissolution of aluminosilicates [38]. The second process may be associated with the alkali-activated product of GGBFS, which is typically eclipsed by the C-A-S-H gel. The existence of Al ions led to enhanced polymerization and notable cross-linking among the C–S–H chains. Furthermore, the third method for enhancing the strength of the mortar involved the formation of the N-A-S-H type gel. Certainly, the N-A-S-H was a small secondary product that existed alongside the main composition domain of the C–S–H gel category [39]. This may enhance compressive properties by boosting gel density through a decrease in total porosity volume [40].

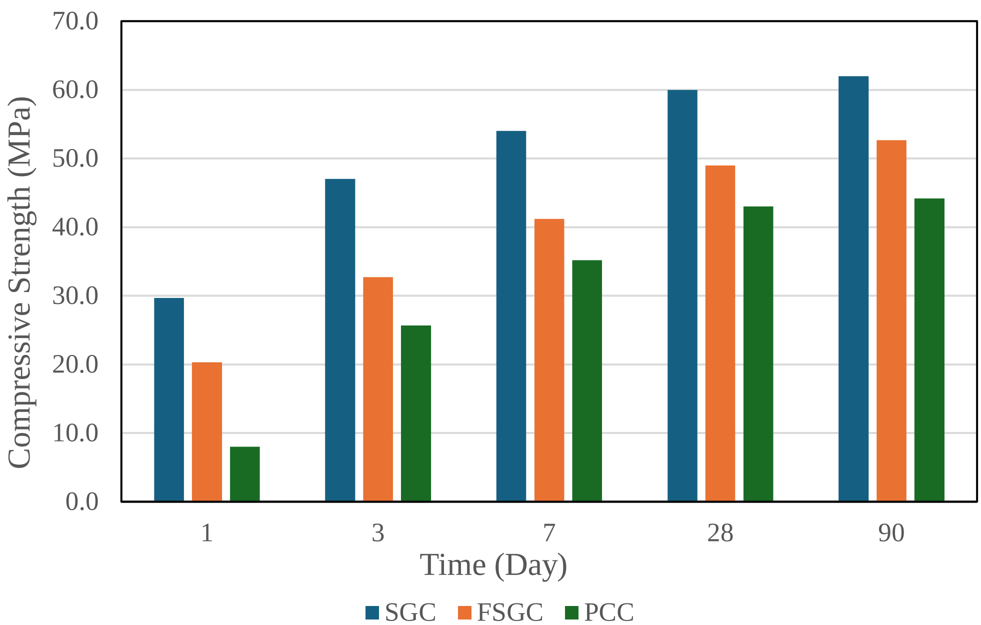

Fig 10. Compressive Strength development for concrete mixes with time

3.3. Flexural Strength (f_r)

f_r test was performed on 150×150×500 mm prismatic specimens. The test was carried out under three-point loading configuration according to ASTM C293 standard [28]. Three sets of specimens of each mix were tested for each of the curing age and their average is reported. All specimens failed with a crack initiated at the mid span right under loading location and propagated up to the compression side of the specimen as shown in Fig 11. The modulus of rupture of GPC was found to be lower than that of Portland cement concrete, as shown in Fig 12. At the age of 28 days, the modulus of rupture for PCC is higher than the modulus of rupture for SGC and FSGC by a percentage of 26.9% and 45.8% respectively. While the modulus of rupture for SGC is higher than that of FSGC by a percentage of 14.9% at the age of 28 days. Similar trends in the f_r development were also observed at ages of 3 and 7 days. The observed enhancement in the f_r of the GPC containing higher GGBFS content could mainly be attributed to the increment in the CaO level in the concrete network as explain widely in section 3.2.

The f_t of concrete relies on the cohesion (c) between the cementitious materials and aggregate particles, as well as the friction angle (ϕ) at both micro and macro cracks [41]. Consequently, the f_t of concrete is greatly influenced by the cohesion characteristics of the binder. While the literature lacks dependable data for (c) of GPC, it can be presumed that the value of (c) for GPC is lower compared to that of PCC, as demonstrated through microstructure analysis.

Fig 11. Failure mode of flexural strength test

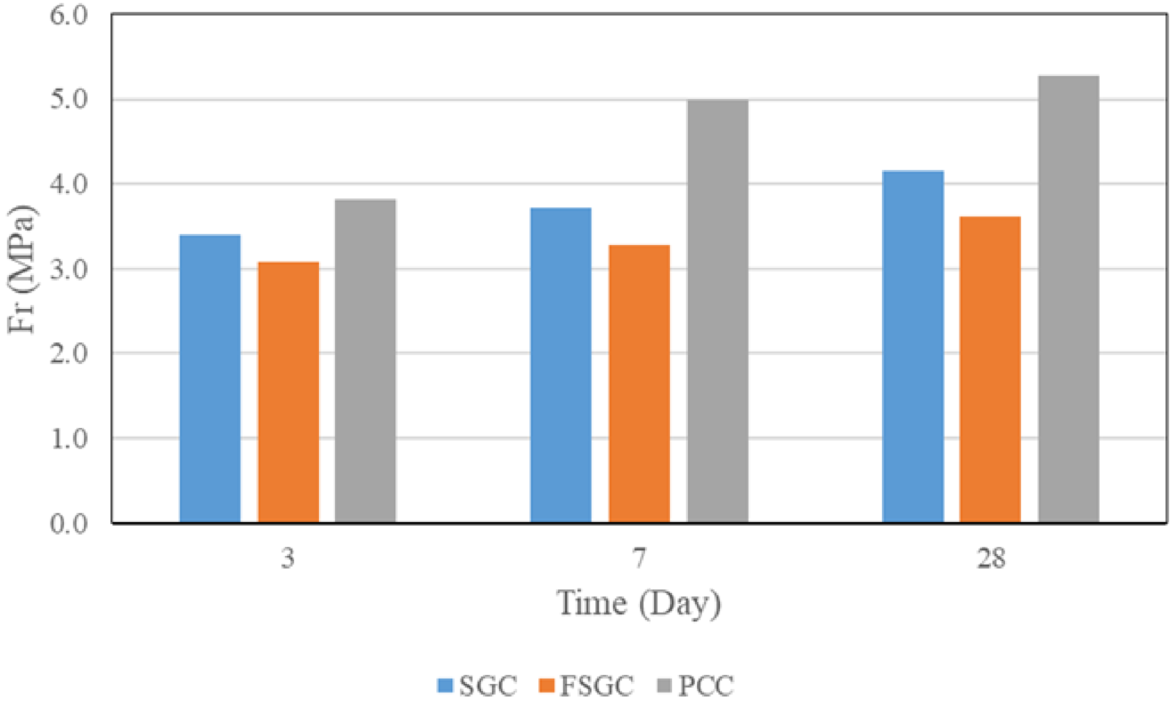

Fig 12. Flexural Strength test results

3.4. Indirect splitting tensile Strength

The indirect splitting tensile strength test was conducted in accordance with the ASTM C496 standard [29] using cylindrical specimens with a diameter of 150 mm and a height of 300 mm, applying a diametral compressive force along the length of the cylindrical concrete specimen until failure happened. For each curing age, three sets of samples from each mix were tested, and their average results are presented.

All specimens failed by a crack initiated at the middle of cross section of the specimen and propagated until the specimen is separated into two halves as shown in Fig 13. The f_t of GPC was found to be lower than that of Portland cement concrete, as shown in Fig 14. At the age of 28 days, the f_t for PCC is higher than the splitting tensile strength for SGC and FSGC by a percentage of 26.7% and 50.0% respectively. While the f_t for SGC is higher than that of FSGC by a percentage of 15.6% at the age of 28 days. Similar trends in f_t development were also observed at ages of 3 and 7 days. It can be observed that the GPC achieved a lower indirect splitting f_t than the PCC which was in contrast for the case of f_c while compatible with f_r test results. This conclusion about the indirect splitting f_t of GPC and PCC aligns with several earlier studies [42], [43], and [44]. Microstructure analysis could validate these findings.

Fig 13. Failure mode of indirect splitting tensile

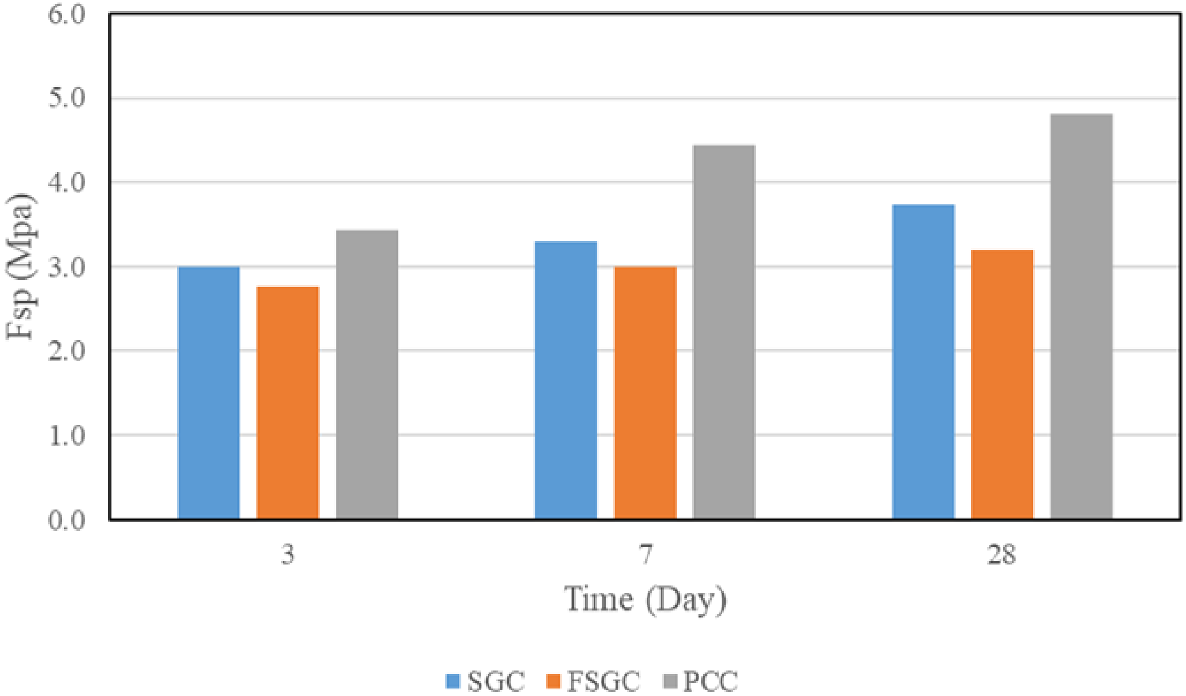

Fig 14. Indirect splitting tensile strength test results

3.5. Bond strength (Pullout)

Pullout test was carried out to study the bond strength between concrete and reinforcing steel bars according to previous studies [30], [25]. Concrete cylinders of diameter 100 mm and length of 200 mm were used. Each specimen was reinforced by 12 mm diameter ribbed reinforcing bar with a yield strength of 557 MPa, a tensile strength of 716 MPa and an elongation percentage of 21.0%. The bonded length of the reinforcing steel bars was seven times the bar diameter with a value of 8.4 cm. The results of the specimens failed with sliding of the reinforcement bars were taken into account while the specimens failed with rupture of concrete cylinders were excluded. Fig 15 shows that sliding mode of failure of pull out test. The pull out bond strength of a steel reinforcing bar installed in the concrete is plotted in Fig 16. It has been observed that the bond strength of GPC mixes were much higher than the bond strength of Portland cement concrete mix by a percentage of 62 % for SGC mix and 52% for FSGC mix after 28 days. Similar trends in bond strength were also observed at ages of 3 and 7 days. The higher bond strength of the reinforcement bars with the geopolymer mixes compared to that of PCC mix could be attributed to the higher confinement properties of geopolymer mixes due to higher f_c.

Fig 15. Failure mode of Pull-out test

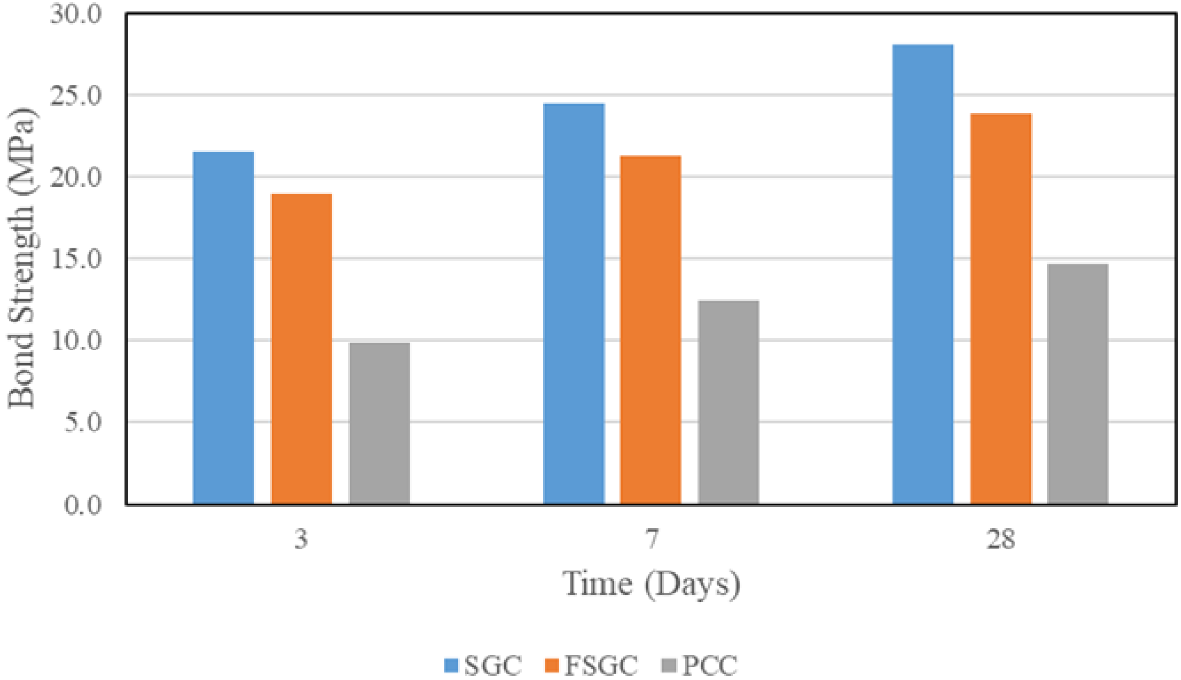

Fig 16. Pull out test results

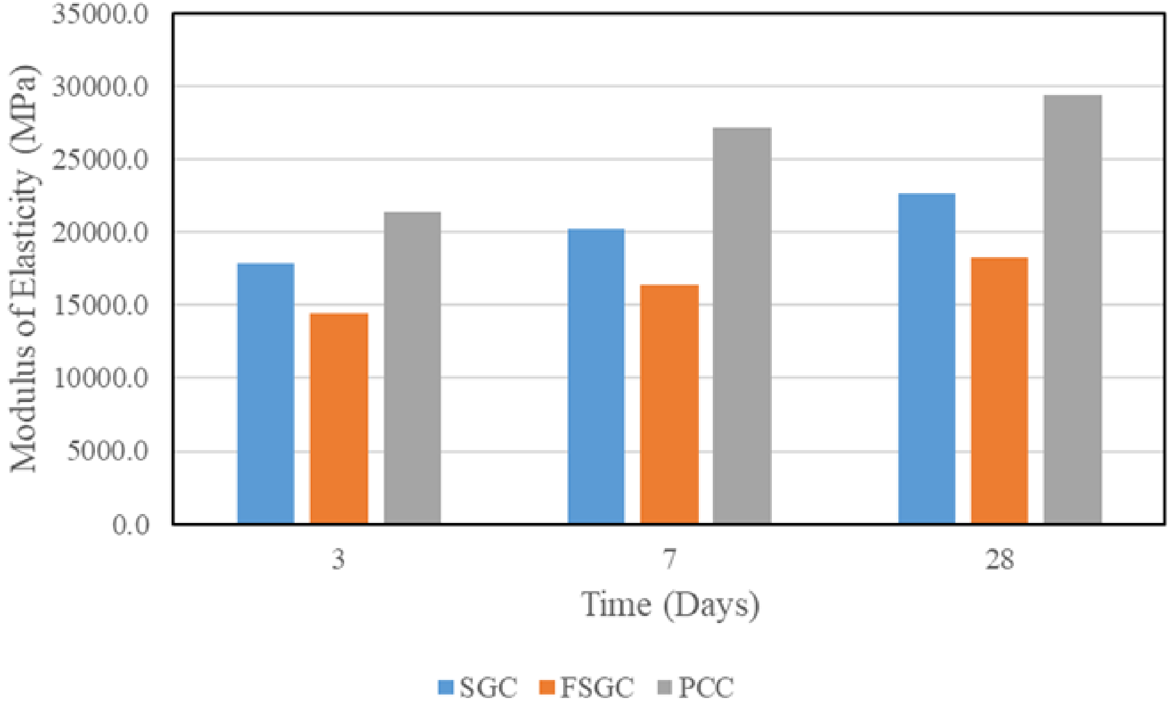

Fig 17. Modulus of elasticity test results

3.6. Modulus of elasticity (E)

The *E* for all mixtures was assessed using concrete cylinders measuring 150 mm in diameter and 300 mm in length, following the ASTM C469 standard [31]. It is a compression test where a load is applied using a Constant-Rate of-Traverse (CRT) machine until a specified stress level is achieved. The *E* value has been established within the working stress range (0 to 40% of ultimate strength). To ensure consistency, ASTM C469 recommends conducting a minimum of two consecutive loadings, and if the measurements are consistent, they may be averaged. Figure 17 displays the *E* results for the three tested mixes. Studies have shown that GPC mixtures resulted in *E* that was 28.4% lower for SGC mixes and 39.1% lower for FSGC mixes compared to Portland cement concrete after a curing period of 28 days. Comparable patterns in the *E* were noted at both 3 and 7 days of age.

3.7. Stress-Strain relationship

The experimental stress-strain response in compression of concrete specimens after 28 days was conducted on cylindrical samples measuring 150 mm in diameter and 300 mm in height. The axial strains have been calculated using the average of 2 Linear Variable Displacement Transformers (LVDTs) and 2 strain gauge readings that assess the overall deformation across the entire height of the specimen. It was noted that the rising segment of the stress-strain curves for SGC, FSGC, and PCC concrete was nearly linear up to the peak stress and then failed in a brittle manner right after reaching the peak stress, as shown in Fig 18. Upon attaining maximum stress, the SGC and FSGC concrete exhibited a quicker decrease in the descending portion of the stress-strain curves. Nevertheless, PCC concrete exhibited a softening reduction in the descending part of the stress-strain curves. Atis et al. [45] and Nabeel et al. [46] also reported a rise in the brittleness of GPC. This behavior of GPC can be ascribed to the significant micro-cracking in SGC and FSGC concrete [47]. Table 5 shows the maximum stress and strain at maximum stress derived from the stress-strain curve for all concrete mixtures.

Table 5 Peak stress and strain at peak stress of tested specimens in compression after 28 days

Mixes	Peak Stress (MPa)	Strain at peak stress
SGC	48.36	0.0025
FSGC	38.48	0.0024
PCC	36.15	0.0019

The *E* was additionally derived from the experimental stress-strain characteristics in compression to compare the results of *E* determined from stress-strain behavior in compression with the values measured in the *E* test conducted according to ASTM C469 and detailed in section (3.6). As per ACI 318-11, the *E* is defined as the slope of the secant line of a stress-strain graph extending from the origin to the point where stress equals 40% of the maximum stress.

Fig 18. Failure mode of compression stress strain test

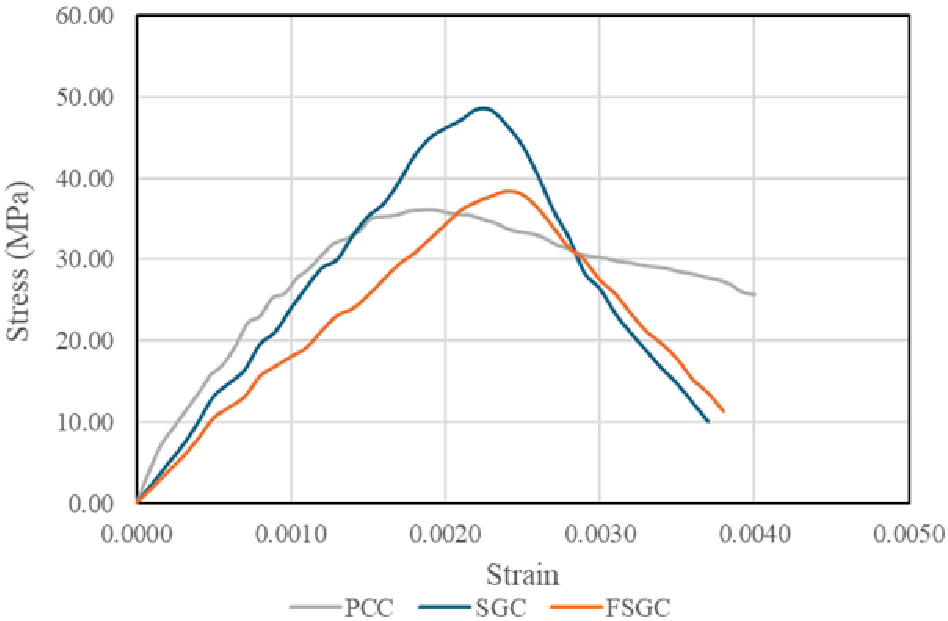

Fig 19. Stress strain curve relationship for concrete mixes

Figs 20, 21, and 22 display the stress-strain curve for each mix separately, with the secant modulus shown on each curve along with its slope equation and correlation coefficient. Table 6 presents the *E* value obtained after 28 days for each blend, measured using the ASTM C496 test and calculated from the compression stress-strain relationship. It has been noted that GPC exhibits a lower *E* compared to Portland cement concrete, aligning with the findings of Yang et al. [48] and Douglas et al. [23], who indicated that alkali-activated concrete typically has a lower *E* than OPC concrete with comparable f_c. The reduced *E* in geopolymer mixes may be explained by their decreased f_t, as during the test the concrete sample experiences lateral tensile forces that could lead to quicker micro cracking of the specimen in contrast to PCC specimens.

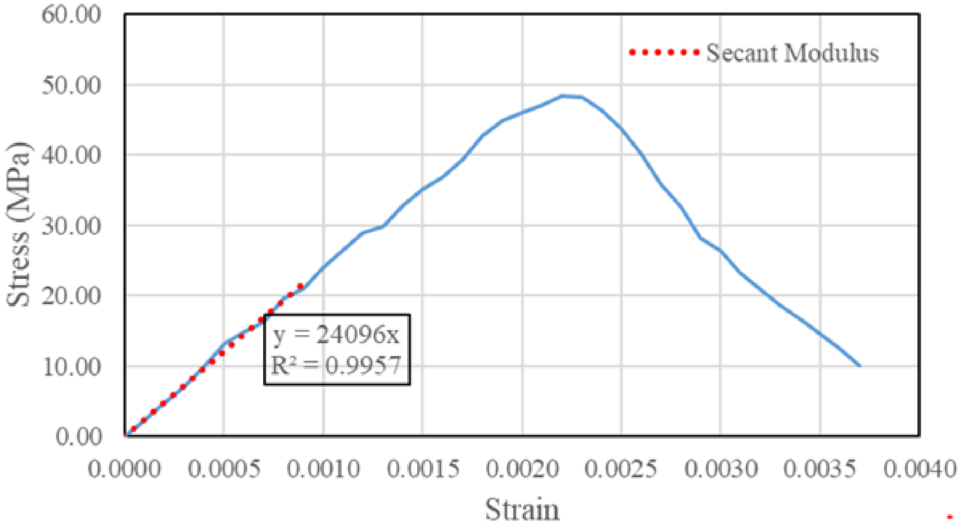

Fig 20. Stress strain curve relationship and secant modulus for SGC mix

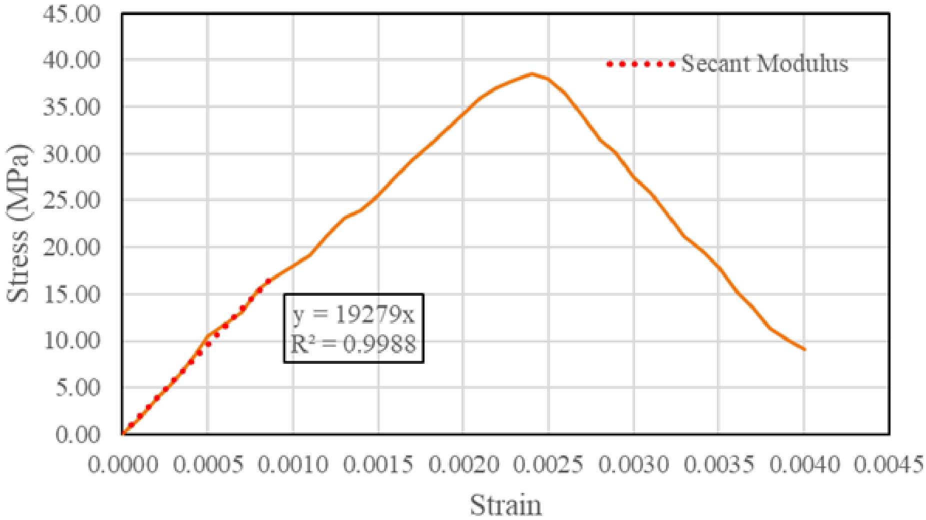

Fig 21. Stress strain curve relationship and secant modulus for FSGC mix

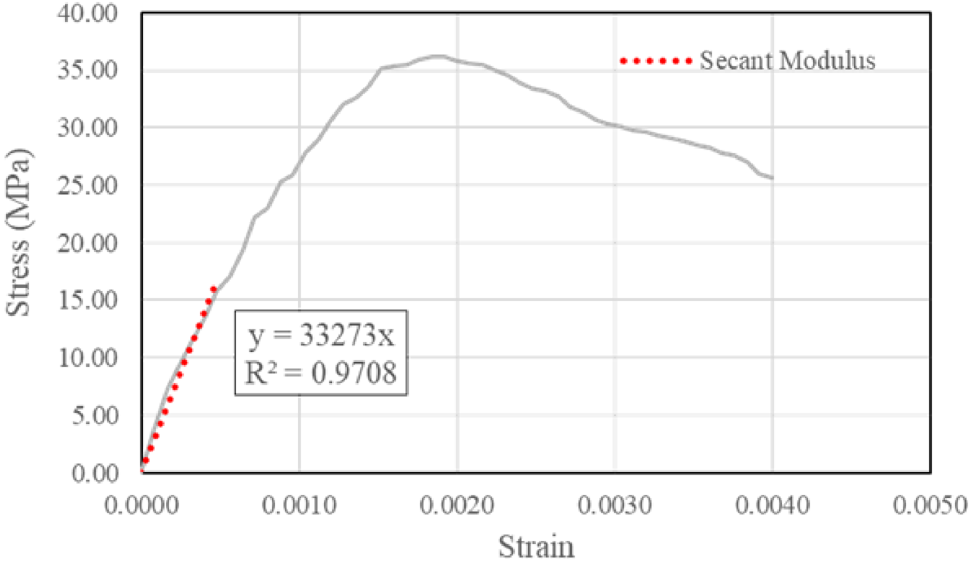

Fig 22. Stress strain curve relationship and secant modulus for PCC mix

Table 6 Comparison between moduli of elasticity from three methods. (E_1) is the calculated *E* from stress-strain behavior in compression, (E_2) is the measured *E* from test that has been performed according to ASTM C469 and (E_3) is the predicted *E* based on ACI318 equation.

Mixes	E_1 (MPa)	E_2 (MPa)	E_3 (MPa)
SGC	23971	22655	32562
FSGC	19452	18280	29426
PCC	30504	29378	27566

3.8. Coefficient of Thermal Expansion (CTE)

The coefficient of thermal expansion (CTE) was measured in accordance with the ASTM C531 standard [32]. The specimens measuring 70×70×285 mm, with studs on both ends, had their length changes recorded after being cured in a controlled environment at 20 °C and 92% relative humidity for 24 hours, followed by heating in an oven at 100 °C for an additional 24 hours. The CTE was calculated as stated in the ASTM C531 standard [32] by dividing the change in length by the change in temperature. The CTE is expressed in macrostrains per unit temperature since the length alteration from thermal expansion was minimal. Table 7 presents a summary of the CTE results for the concrete mixes that were tested. Research has shown that GPC mixtures exhibit a 50.7% lower coefficient of thermal expansion compared to Portland cement concrete for the SGC mix, and a 38.0% reduction for the FSGC mix. These findings are consistent with those reported by M.S. Eisa et al. [49]

Table 7 Coefficient of thermal expansion results

Mixes	PCC				SGC				FSGC			
Specimens	1	2	3	4	1	2	3	4	1	2	3	4
Length @ 20° (mm)	285	284	285	283	284	284	285	285	283	285	286	285
CRD_{20} (mm)	3.503	2.863	3.962	1.896	1.561	1.780	1.302	1.250	1.405	1.321	1.103	1.609
CRD_{100} (mm)	3.756	3.106	4.185	2.105	1.670	1.901	1.405	1.389	1.556	1.467	1.238	1.752
CTE (μ-strain/°C)	11.09	10.69	9.78	9.23	4.79	5.32	4.51	6.09	6.67	6.40	5.90	6.27
Average CTE (μ-strain/°C)	10.19				5.17				6.31			

CRD_{20}: Comparator Reading at 20 ºC
CRD_{100}: Comparator Reading at 100 ºC
CTE: Coefficient of Thermal Expansion

3.9. Drying Shrinkage

Drying shrinkage was conducted on prisms of dimensions 70×70×285 mm as per ASTM C596 standard [33]. The length of samples measured after 24 hours of curing as the initial comparator reading for PCC and GPC specimens (CRDi). The specimens were maintained at room temperature, and comparator readings were collected after 4, 11, 18, and 25 days, as well as 56 days of air storage (CRDf). The length change at each age of air drying was estimated using the ASTM C596 standard. [33] and expressed in micro-strain of gage length as shown in. Tables 8.1, 8.2 and 8.3 summarize the results of drying shrinkage for tested concrete mixes. Also, Fig 23 represents the results that has been summarized in tables 8. It has been observed that GPC mixes achieves lower drying shrinkage than Portland cement concrete mix.

Table 8.1 Drying shrinkage of PCC mix

Mixes	PCC										
Specimens	CRD_i (mm)	CRD_f (mm)					Average shrinkage (μ-train/°C)				
Age (Day)		4	11	18	25	56	4	11	18	25	56
1	-0.321	-0.326	-0.370	-0.375	-0.377	-0.378	477.19	582.45	665.79	678.94	681.58
2	0.412	0.205	0.156	0.113	0.112	0.111					
3	0.520	0.269	0.213	0.178	0.177	0.177					
4	0.313	0.268	0.261	0.249	0.238	0.237					

CRD_i: Initial Comparator Reading
CRD_f: Final Comparator Reading

Table 8.2 Drying shrinkage of SGC mix

Mixes	SGC									
Specimens	CRD$_i$ (mm)	CRD$_f$ (mm)					Average shrinkage (µ-train/°C)				
Age (Day)		4	11	18	25	56	4	11	18	25	56
1	-0.551	-0.593	-0.611	-0.621	-0.623	-0.624	190.35	238.60	261.40	268.42	271.05
2	-0.713	-0.795	-0.806	-0.808	-0.811	-0.811					
3	-0.469	-0.509	-0.521	-0.529	-0.531	-0.532					
4	-0.332	-0.385	-0.399	-0.405	-0.406	-0.407					

CRD$_i$: Initial Comparator Reading
CRD$_f$: Final Comparator Reading

Table 8.3 Drying shrinkage of FSGC mix

Mixes	FSGC									
Specimens	CRD$_i$ (mm)	CRD$_f$ (mm)					Average shrinkage (µ-train/°C)				
Age (Day)		4	11	18	25	56	4	11	18	25	56
1	-0.634	-0.682	-0.703	-0.714	-0.716	-0.718	250.82	330.31	370.62	375.98	380.22
2	-0.820	-0.914	-0.927	-0.929	-0.933	-0.933					
3	-0.539	-0.585	-0.599	-0.608	-0.611	-0.612					
4	-0.382	-0.443	-0.459	-0.466	-0.467	-0.468					

CRD$_i$: Initial Comparator Reading
CRD$_f$: Final Comparator Reading

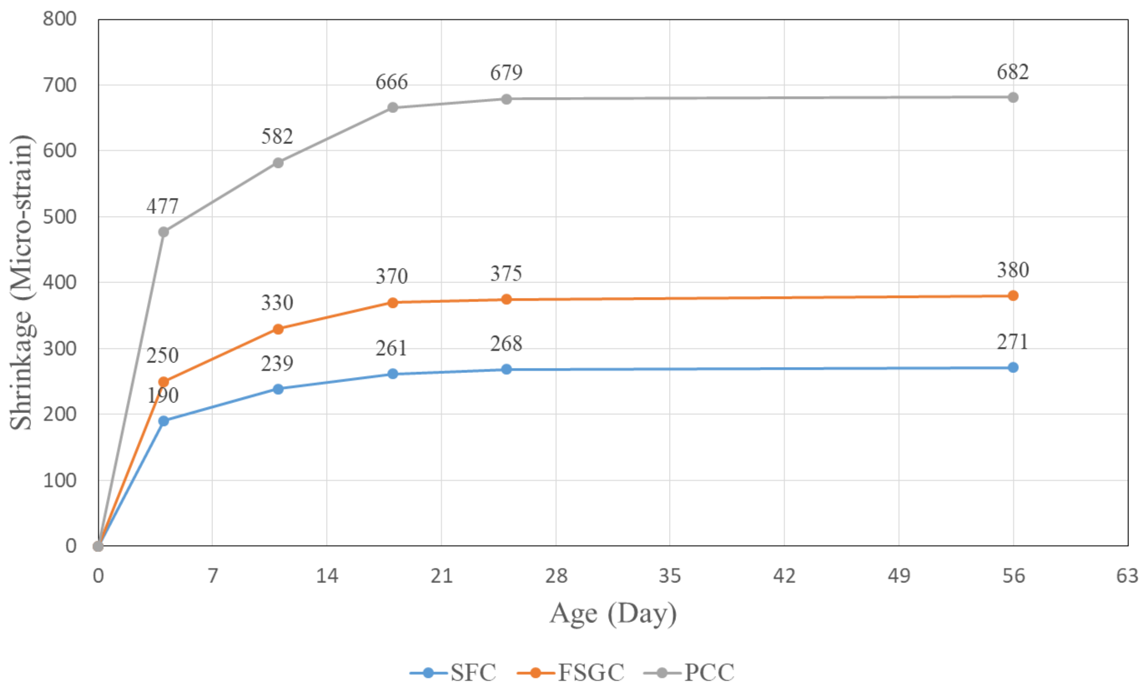

Fig 23. Drying Shrinkage test results

3.10. Microstructure Analysis

Microstructure analysis was conducted on samples from each concrete mix to explain the poor performance of GPC in f_t and f_r, even though it exhibits greater f_c compared to Portland cement concrete. The microscopic features of the primary materials (FA, GGFBS) utilized in the creation of FSGC and SGC concrete indicate that FA is predominantly made up of glassy, spherical particles, facilitating easy flow and mixing in formulations. The particle surfaces seem dense and polished. The particles of GGBS are primarily characterized by distinct edges and angular forms. Thus, their mixtures in cementitious improve the mechanical properties. Conversely, the uneven particle shape negatively impacts the flow characteristics of the cementitious composites. [50], [51].

At a magnification of 1000 x, the FSGC mix exhibits more cracks than the SGC and PCC mixes, as illustrated in Fig 24 and Fig 25. Furthermore, at 8000 x magnification, the FSGC mix had more micro fractures in the interfacial transition zone between coarse aggregate and fly ash paste than the SGC and PCC mixes.

At a magnification of 1000 x, SGC mix has more cracks than PCC mix. Furthermore, at 8000 x magnification, SGC mix revealed more micro fractures in the interfacial transition zone between coarse aggregate and slag paste than PCC mix, as shown in Fig 25 and Fig 26. Due to a rapid reaction between the alkaline activator and GGBS particles in the first phase, small micro fractures occurred in the interfacial transition zone of the SGC mix compared to the FSGC mix [46].
That may be attributed to the fact that FSGC mix has the highest initial slump value among used concrete mixes which is higher than SGC mix by a percentage of 28.5% and higher than PCC mix by a percentage of 270%. while SGC has higher initial slump value than PCC mix but lower slump loss with time than FSGC mix. Nonetheless, the microstructural progression of OPC concrete resulted in denser and more uniform microstructures compared to FSG C and SGC concrete. Fewer unreacted OPC particles and nearly no cracks were noticed in the OPC matrices.

Micro cracks appeared in the microstructure of SGC and FSGC mixes proves that why FSGC mix has the lowest ratio of f_t or f_r to the square root of f_c at 28 days which were 0.51 and 0.57 respectively. While SGC mix has slightly higher ratio of f_t or f_r to f_c at 28 days than FSGC mix which were 0.53 and 0.60 respectively. PCC mix has the highest f_t or f_r to f_c at 28 days than FSGC and SGC mixes which were 0.81 and 0.90 respectively and that may be attributed to the fact that almost no micro cracks were observed at the interfacial transition zone between coarse aggregate and cement paste. The results shown in this study align with those noted in a limited number of earlier studies. [20,46,48].

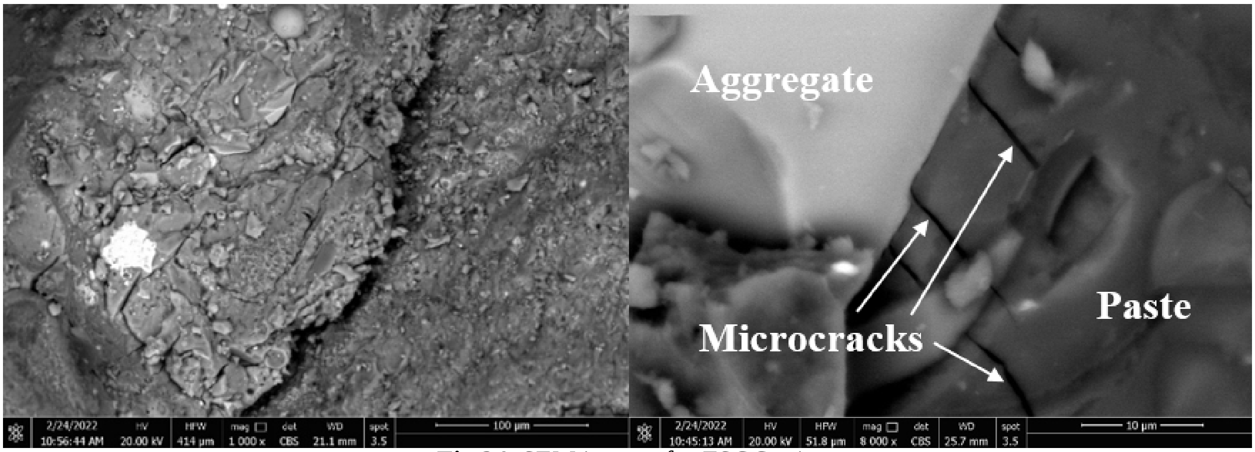

Fig 24. SEM images for FSGC mix

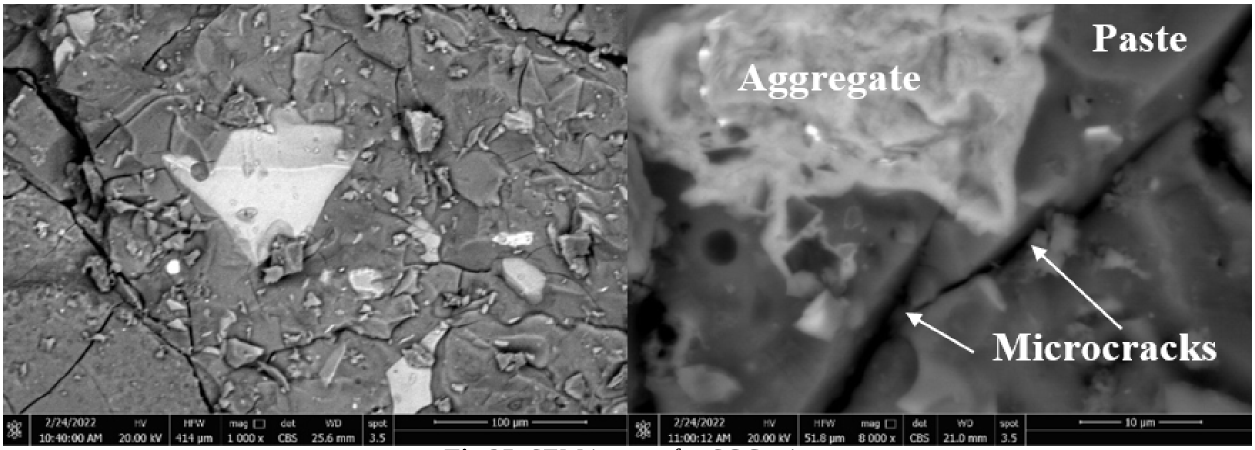

Fig 25. SEM images for SGC mix

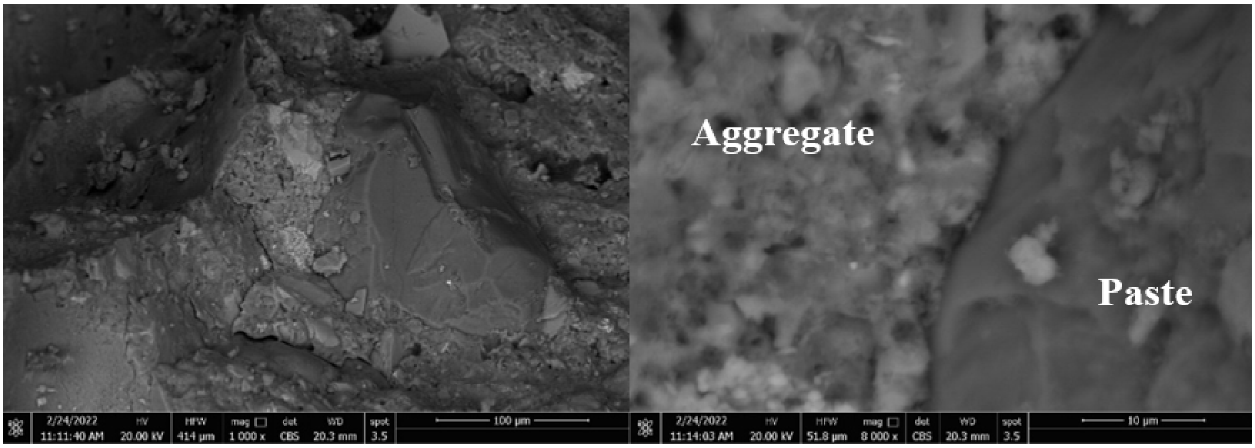

Fig 26. SEM images for PCC mix

4. Conclusions

This study examines the engineering characteristics of FSGC and SGC concrete and compares them to those of PCC. The subsequent conclusions can be made based on the test results.

1. The strength of geopolymerization can be improved through the addition of GGBFS, as higher calcium concentrations were identified as the reason for the increased dissolution and deposition of Al_2O_3 and SiO_2.
2. The 90-day f_c of SGC and FSGC mixtures showed an increase of approximately 3-7% when compared to the 28-day f_c, suggesting that the 28-day f_c can be regarded as the characteristic f_c for GPC.
3. GPC mixes cured at ambient temperature have higher f_c by 40% and higher pull out strength by 91% than PCC. In addition, GPC mixes exhibited lower f_r by 26%, indirect splitting tensile strength by 23% and elastic modulus by 23% than those of conventional concrete at the same binder content due to micro cracks appeared at the microstructure scale of the mixes. The tensile behavior of the GPC may be enhanced using fiber reinforcement.
4. GPC mixtures demonstrated a faster reduction in the descending part of the stress-strain curves. Nevertheless, PCC concrete exhibited gradual softening in the descending section of the stress-strain curves. This characteristic of GPC can be linked to the significant micro-cracking found in SGC and FSGC concrete mixtures.
5. GPC mixes achieved lower coefficient of thermal expansion by 43% and lower drying shrinkage by 52% than conventional concrete, proving that it can be used as a potential retrofitting material for ordinary reinforced concrete structure.
6. The analysis of the microstructure indicates significant microcracking in GPC mixtures when compared to Portland cement concrete, demonstrating the poor performance of GPC mixes under tensile stresses.

References

[1] F. Pacheco-Torgal, Z. Abdollahnejad, A.F. Camões, M. Jamshidi, Y. Ding, Durability of alkali-activated binders: A clear advantage over Portland cement or an unproven issue?, Constr Build Mater. 30 (2012) 400–405.
[2] A.S. Pinto, M. Bustamante, K. Kisselle, R. Burke, R. Zepp, L.T. Viana, R.F. Varella, M. Molina, Soil emissions of N2O, NO, and CO2 in Brazilian Savannas: Effects of vegetation type, seasonality, and prescribed fires.
[3] J. Wang, Y. Dai, L. Gao, Exergy analyses and parametric optimizations for different cogeneration power plants in cement industry, Appl Energy. 86 (2009) 941–948.
[4] G.G. Mejeoumov, Improved cement quality and grinding efficiency by means of closed mill circuit modeling, Undefined. (2009).
[5] P. v. Nidheesh, M.S. Kumar, An overview of environmental sustainability in cement and steel production, J Clean Prod. 231 (2019) 856–871.
[6] P. Chindaprasirt, U. Rattanasak, Improvement of durability of cement pipe with high calcium fly ash geopolymer covering, Undefined. 112 (2016) 956–961.
[7] M.M. Hossain, M.R. Karim, M.K. Hossain, M.N. Islam, M.F.M. Zain, Durability of mortar and concrete containing alkali-activated binder with pozzolans: A review, Constr Build Mater. 93 (2015) 95–109.
[8] A.R.G. Azevedo, D. Cecchin, D.F. Carmo, F.C. Silva, C.M.O. Campos, T.G. Shtrucka, M.T. Marvila, S.N. Monteiro, Analysis of the compactness and properties of the hardened state of mortars with recycling of construction and demolition waste (CDW), Undefined. 9 (2020) 5942–5952.
[9] B.C. McLellan, R.P. Williams, J. Lay, A. van Riessen, G.D. Corder, Costs and carbon emissions for geopolymer pastes in comparison to ordinary portland cement, J Clean Prod. 19 (2011) 1080–1090.
[10] R. D.B, S. PatilH., GEOPOLYMER CONCRETE: A CONCRETE OF NEXT DECADE, Undefined. (2010).

[11] D. Van Dao, H.B. Ly, S.H. Trinh, T.T. Le, B.T. Pham, Artificial Intelligence Approaches for Prediction of Compressive Strength of Geopolymer Concrete, Materials 2019, Vol. 12, Page 983. 12 (2019) 983.
[12] I. Ismail, S.A. Bernal, J.L. Provis, R. San Nicolas, D.G. Brice, A.R. Kilcullen, S. Hamdan, J.S.J. Van Deventer, Influence of fly ash on the water and chloride permeability of alkali-activated slag mortars and concretes, Constr Build Mater. 48 (2013) 1187–1201.
[13] M.M. Al-mashhadani, O. Canpolat, Y. Aygörmez, M. Uysal, S. Erdem, Mechanical and microstructural characterization of fiber reinforced fly ash based geopolymer composites, Constr Build Mater. 167 (2018) 505–513.
[14] G.F. Huseien, J. Mirza, M. Ismail, S.K. Ghoshal, M.A.M. Ariffin, Effect of metakaolin replaced granulated blast furnace slag on fresh and early strength properties of geopolymer mortar, Ain Shams Engineering Journal. 9 (2018) 1557–1566.
[15] G.F. Huseien, J. Mirza, M. Ismail, M.W. Hussin, Influence of different curing temperatures and alkali activators on properties of GBFS geopolymer mortars containing fly ash and palm-oil fuel ash, Constr Build Mater. 125 (2016) 1229–1240.
[16] T. Phoo-Ngernkham, V. Sata, S. Hanjitsuwan, C. Ridtirud, S. Hatanaka, P. Chindaprasirt, High calcium fly ash geopolymer mortar containing Portland cement for use as repair material, Constr Build Mater. 98 (2015) 482–488.
[17] E. Vasconcelos, S. Fernandes, B. De Aguiar, F. Pacheco-Torgal, Concrete retrofitting using CFRP and geopolymer mortars, Materials Science Forum. 730–732 (2013) 427–432.
[18] R.J. Thomas, S. Peethamparan, Alkali-activated concrete: Engineering properties and stress–strain behavior, Constr Build Mater. 93 (2015) 49–56.
[19] S. Popovics, A numerical approach to the complete stress-strain curve of concrete, Cem Concr Res. 3 (1973) 583–
[20] F. Collins, J.G. Sanjayan, Microcracking and strength development of alkali activated slag concrete, Cem Concr Compos. 23 (2001) 345–352.
[21] Y. Ding, J.G. Dai, C.J. Shi, Mechanical properties of alkali-activated concrete: A state-of-the-art review, Constr Build Mater. 127 (2016) 68–79.
[22] K.H. Yang, A.R. Cho, J.K. Song, Effect of water–binder ratio on the mechanical properties of calcium hydroxide-based alkali-activated slag concrete, Constr Build Mater. 29 (2012) 504–511.
[23] E. Douglas, A. Bilodeau, V.M. Malhotra, Properties and Durability of Alkali-Activated Slag Concrete, Materials Journal. 89 (1992) 509–516.
[24] A.A. Aliabdo, A.E.M. Abd Elmoaty, M.A. Emam, Factors affecting the mechanical properties of alkali activated ground granulated blast furnace slag concrete, Constr Build Mater. 197 (2019) 339–355.
[25] I. Amer, M. Kohail, M.S. El-Feky, A. Rashad, M.A. Khalaf, Characterization of alkali-activated hybrid slag/cement concrete, Ain Shams Engineering Journal. 12 (2021) 135–144.
[26] ASTM C143/C143M − 15a "Standard Test Method for Slump of Hydraulic-Cement Concrete," (n.d.). https://doi.org/10.1520/C0143_C0143M-15A.
[27] B. S. EN, "12390-3. Testing hardened concrete–Part 3: Compressive strength of test specimens," Br. Stand. Inst., 2002., (n.d.).
[28] ASTM C293 "Standard Test Method for Flexural Strength of Concrete Using Simple Beam With Center-Point Loading," (n.d.).
[29] ASTM C496 "Standard Test Method for Splitting Tensile Strength of Cylindrical Concrete Specimens," (n.d.).
[30] A.M. Fernández-Jiménez, A. Palomo, C. López-Hombrados, Engineering Properties of Alkali-Activated Fly Ash Concrete, Materials Journal. 103 (2006) 106–112.
[31] ASTM C469 "Standard Test Method for Static Modulus of Elasticity and Poisson's Ratio of Concrete in Compression," (n.d.).
[32] ASTM C531 "Standard Test Method for Linear Shrinkage and Coefficient of Thermal Expansion of Chemical-Resistant Mortars, Grouts, Monolithic Surfacings, and Polymer Concretes," (n.d.).
[33] ASTM C596 "Standard Test Method for Drying Shrinkage of Mortar Containing Hydraulic Cement," (n.d.).
[34] M.H. Al-Majidi, A. Lampropoulos, A. Cundy, S. Meikle, Development of geopolymer mortar under ambient temperature for in situ applications, Constr Build Mater. 120 (2016) 198–211.
[35] T. Phoo-Ngernkham, A. Maegawa, N. Mishima, S. Hatanaka, P. Chindaprasirt, Effects of sodium hydroxide and sodium silicate solutions on compressive and shear bond strengths of FA–GBFS geopolymer, Constr Build Mater. 91 (2015) 1–8.
[36] S. Kumar, R. Kumar, S.P. Mehrotra, Influence of granulated blast furnace slag on the reaction, structure and properties of fly ash based geopolymer, J Mater Sci. 45 (2010) 607–615.
[37] S. Puligilla, P. Mondal, Role of slag in microstructural development and hardening of fly ash-slag geopolymer, Cem Concr Res. 43 (2013) 70–80.
[38] H.M. Khater, Effect of Calcium on Geopolymerization of Aluminosilicate Wastes, Journal of Materials in Civil Engineering. 24 (2012) 92–101.
[39] R.J. Myers, S.A. Bernal, R. San Nicolas, J.L. Provis, Generalized structural description of calcium-sodium aluminosilicate hydrate gels: The cross-linked substituted tobermorite model, Langmuir. 29 (2013) 5294–5306.
[40] Z. Li, S. Liu, Influence of Slag as Additive on Compressive Strength of Fly Ash-Based Geopolymer, Journal of Materials in Civil Engineering. 19 (2007) 470–474.
[41] J. Munro, Limit analysis and concrete plasticity M. P. Nielsen Prentice-Hall, Englewood Cliffs, NJ, USA, 1984, 420 pp.,£40.80, 1985. https://www.routledge.com/Limit-Analysis-and-Concrete-Plasticity/Nielsen-Hoang/p/book/9781439803967 (accessed March 25, 2022).
[42] M. Sofi, J.S.J. Van Deventer, P.A. Mendis, G.C. Lukey, Bond performance of reinforcing bars in inorganic polymer concrete (IPC), J Mater Sci. 42 (2007) 3107–3116.
[43] D. Hardjito, B. Rangan, DEVELOPMENT AND PROPERTIES OF LOW-CALCIUM FLY ASH-BASED GEOPOLYMER CONCRETE, Undefined. (2005).
[44] M. Albitar, P. Visintin, M.S. Mohamed Ali, M. Drechsler, Assessing behaviour of fresh and hardened geopolymer concrete mixed with class-F fly ash, KSCE Journal of Civil Engineering. 19 (2015) 1445–1455.

[45] C. Duran Atiş, C. Bilim, Ö. Çelik, O. Karahan, Influence of activator on the strength and drying shrinkage of alkali-activated slag mortar, Constr Build Mater. 23 (2009) 548–555.
[46] N.A. Farhan, M.N. Sheikh, M.N.S. Hadi, Investigation of engineering properties of normal and high strength fly ash based geopolymer and alkali-activated slag concrete compared to ordinary Portland cement concrete, Constr Build Mater. 196 (2019) 26–42.
[47] N.K. Lee, H.K. Lee, Setting and mechanical properties of alkali-activated fly ash/slag concrete manufactured at room temperature, Constr Build Mater. 47 (2013) 1201–1209.
[48] K.H. Yang, J.K. Song, K.S. Lee, A.F. Ashour, Flow and compressive strength of alkali-activated mortars, ACI Mater J. 106 (2009) 50–58.
[49] M.S. Eisa, M.E. Basiouny, E.A. Fahmy, Effect of metakaolin-based geopolymer concrete on the length of rigid pavement slabs, Innovative Infrastructure Solutions. 6 (2021) 1–9.
[50] A. Castel, S.J. Foster, Bond strength between blended slag and Class F fly ash geopolymer concrete with steel reinforcement, Cem Concr Res. 72 (2015) 48–53.
[51] S. Nagajothi, S. Elavenil, Effect of GGBS Addition on Reactivity and Microstructure Properties of Ambient Cured Fly Ash Based Geopolymer Concrete, Silicon 2020 13:2. 13 (2020) 507–516